Available online at www.sciencedirect.com
SCIENCE DIRECT®
Cement & Concrete Composites 27 (2005) 55–64
Cement & Concrete Composites
www.elsevier.com/locate/cemconcomp

Behavior of SCC confined in short GFRP tubes

H. El Chabib, M. Nehdi *, M.-H. El Naggar

Department of Civil and Environmental Engineering, University of Western Ontario, London, Ont., Canada N6A 5B9

Received 16 July 2003; accepted 10 February 2004

Abstract

While there is abundant research information on ordinary concrete confined in FRP tubes, there is little data on the behavior of self-consolidating concrete (SCC) under such condition. Because of the usually higher total shrinkage and lower coarse aggregate content of SCC compared to that of ordinary concrete, its composite performance under confined conditions needs special investigation. SCC confined in FRP tubes can have unique structural applications. For instance, cast-in-place deep foundations such as drilled shaft piles are often subjected to two sources of problems. First, the integrity and uniformity of the cross-sectional area of these structural elements cannot be assured using normal concrete because of limited accessibility and visibility during construction. Cavities and soil encroachments leading to soil and air pockets can jeopardize the load-bearing capacity of such piles. Second, corrosion problems of steel reinforcement in deep foundations have been costly, requiring annual repair costs of more than $2 billion in the US alone. SCC, which is able to consolidate under its self-weight without vibration, can be cast into GFRP envelopes that act as corrosion-resistant reinforcement to offer an alternative pile construction method that addresses both challenges cited above. To demonstrate the concept, this paper presents results of a laboratory investigation on the behavior of SCC confined in short GFRP tubes and subjected to axial and transverse load, including the effect of using expansive cement and shrinkage-reducing admixtures to enhance the GFRP tube-SCC interfacial contact.

Keywords: Self-consolidating concrete; Fiber-reinforced polymer; Stress–strain; Compression; Bending

1. Introduction

The ultimate load-bearing capacity of cast-in-place concrete piles is significantly affected by the compressive strength of concrete, the pile cross-section, the amount of steel reinforcement and various soil properties. Both the compressive strength of concrete and the integrity of the pile's cross-section depend on the consolidation of fresh concrete during placement.

Generally, concrete is consolidated with mechanical vibrators, a process that is operator-sensitive. In deep concrete piles where accessibility and visibility are limited, consolidation of concrete is particularly difficult. Over-consolidated concrete might segregate or destabilize soil particles around the shaft wall causing it to collapse into the concrete core. Under-consolidated concrete can have voids and cavities, leading to air and soil pockets and exposure of steel reinforcement to corrosion attack. Consequently, the integrity and uniformity of the pile's cross-section cannot be assured, concrete strength is adversely affected and the load-bearing capacity of the pile is jeopardized.

To alleviate both the problem of air cavities and soil pockets in the concrete and corrosion of steel reinforcement, a novel technology for the construction of drilled-shaft concrete piles is proposed in this study. Self-consolidating concrete (SCC), a material that consolidates under its own weight with no vibration and without exhibiting segregation or bleeding, can be used instead of normal concrete to assure the structural integrity and uniformity of the cross-sectional area of deep foundations. Self-consolidating concrete can be cast into a fiber-reinforced polymer (FRP) envelope, which acts as stay-in-place structural formwork. In addition, the FRP envelope acts as a protective jacket in aggressive environments such as in the case of marine piles [1] and piles constructed in soils rich in chloride ions and sulfate salts [2], and may provide total or

* Corresponding author. Tel.: +1-519-661-2111x88308; fax: +1-519-661-3779.
E-mail address: mnehdi@eng.uwo.ca (M. Nehdi).

0958-9465/$ - see front matter © 2004 Elsevier Ltd. All rights reserved.
doi:10.1016/j.cemconcomp.2004.02.045

Nomenclature

Notations

α	winding angle of glass fibers in the FRP tubes
v	Poisson's ratio
Δ_{co}	maximum axial deflection of unconfined cylinders at concrete failure
Δ_{cc}	maximum axial deflection of confined cylinders at concrete failure
Δ_{ult}	ultimate axial deflection of confined cylinders at failure
Δ_{max}	maximum mid-span deflection of specimen subjected to pure bending
ε_{co}	maximum axial strain of unconfined cylinders
ε_{cu}	ultimate axial strain of confined cylinders
ε_c	strain
ASHA	anti-shrinkage admixture
C	cement
D	inside diameter of FRP tubes
E	modulus of elasticity of FRP tubes
E_1	slope of the first linear zone
E_2	slope of the second linear zone
EC	expansive cement
FA	fly ash
f'_c	compressive strength of unconfined concrete specimen
f'_{cu}	ultimate compressive strength of confined concrete specimen
f_0	reference stress (the intersection of the second linear zone with the stress axis)
f_c	stress
G	gravel
GBFS	ground blast furnace slag
GFRP	glass fiber-reinforced polymer
L	length of specimen
NC	normal concrete
NCE	normal concrete with expansive cement and anti-shrinkage admixture
n	curve-shape parameter
OPC	ordinary portland cement
P_{co}	maximum axial load of unconfined cylinder at concrete failure
P_{cc}	maximum axial load of confined cylinder at concrete failure
P_{ult}	ultimate axial load of confined cylinder at failure
P_{max}	maximum transverse load of cylinder subjected to pure bending
S	sand
SCC	self-consolidating concrete
SCCE	self-consolidating concrete with expansive cement and anti-shrinkage admixture
SP	superplasticizer
t	thickness of the GFRP tube
VMA	viscosity-modifying admixture
W	water
W/C	water to cement mass ratio
W/B	water to binder mass ratio

partial replacement for steel reinforcement. More importantly, the FRP tube provides a uniform lateral confinement to the concrete core in piles and significantly enhances the compressive strength of concrete and its ductility [3,4].

The confinement of concrete is the restraint of its lateral deformation under axial loading. Extensive research has been conducted on concrete-filled steel tubes for use as piles and columns [5,6]. However, FRP tubes provide several advantages over steel tubes when used as confining protective jackets for concrete piles. In addition to their high strength-to-weight ratio, FRP materials are known for their high corrosion-resistance. Unlike the confining effect provided by steel tubes, which reaches a threshold value once the steel yields, FRP tubes provide a continuously increasing confining pressure until failure, which adds to both the ultimate compressive strength and ductility of the concrete member [7,8].

The focus of this study is to investigate the confinement effect of glass fiber-reinforced polymer (GFRP) tubes on the strength and ductility of short SCC cylindrical columns subjected to uniaxial compression and transverse loading. Specimens made both of normal concrete (NC) and SCC were tested and their behavior was compared. Moreover, because the interfacial contact between the concrete core and the confining tube is important for achieving a composite behavior, especially under transverse loading, SCC and NC specimens prepared using Type 10 Canadian ordinary portland cement (ASTM Type I) and expansive cement along with a shrinkage-reducing admixture were investigated. Both ends of specimens tested under transverse loading were monitored for any slippage between the concrete and the confining tube. While the behavior of confined ordinary concrete has been well studied and documented, there is a lack of data on the structural performance of confined self-consolidating concrete. SCC is often associated with higher shrinkage and a lower coarse aggregate content compared to that of ordinary concrete, which may affect its behavior under confined conditions. This paper provides valuable data in this area, with special focus on the use of SCC confined in GFRP tubes in deep foundation applications.

2. Experimental procedures

A total of 36 cylindrical specimens were prepared and tested in this study. Eighteen 150×300 mm (6×12 in.) short cylindrical specimens were tested under uniaxial compression to investigate the confinement effect of GFRP on axially loaded normal concrete and self-consolidating concrete made with either ordinary portland cement (OPC) or expansive cement (EC). Eighteen 150×1100 mm (6×43 in.) cylindrical specimens were tested under transverse load to investigate the confinement effect of GFRP tubes on normal concrete and SCC subjected to transverse loading along the effect of using expansive cement and a shrinkage-reducing admixture on the interfacial contact and slippage between the concrete and the confining tube.

Short cylindrical specimens tested in compression included six plain concrete control cylinders (three NC and three SCC) and 12 concrete cylinders confined by GFRP tubes. The confined specimens included three cylinders made of normal concrete using OPC, three cylinders made of SCC using OPC, and three cylinders of each (NC and SCC) made using expansive cement. Similarly, the specimens tested under transverse load included six plain concrete control specimens (three NC and three SCC) and 12 specimens confined in GFRP tubes (3-OPC-NC, 3-OPC-SCC, 3-expansive-cement-NC and 3-expansive-cement-SCC).

2.1. Materials

Concrete specimens were prepared from four different concrete mixtures designed to achieve similar 28-day compressive strengths. Proportions of concrete mixtures and their corresponding properties are shown in Tables 1 and 2, respectively. Canadian Type 10 OPC (ASTM Type I) was used to prepare the normal concrete (NC) mixture. The SCC mixture was prepared using the same type of cement incorporating proportions of fly ash (FA) and ground granulated blast furnace slag (GBFS) along with a superplasticizer and a viscosity-modifying admixture (VMA). Two other concrete mixtures (NCE and SCCE) having the same proportions as the NC and SCC mixtures were prepared using expansive cement (EC) instead of Type 10 OPC in addition to a commercial shrinkage-reducing admixture. Anhydrous tetracalcium trialuminate sulfate expansive cement was used. GFRP tubes consisted of a filament-wound bi-directional glass-fiber oriented at ±55° with respect to the longitudinal axis of the tube. They had an inside diameter of 150 mm (6 in.) and a uniform thickness of 6 mm (0.23 in.). The physical and mechanical properties of the GFRP tubes are listed in Table 3.

2.2. Specimen preparation and testing procedures

2.2.1. Cylindrical specimens under compression

Plain concrete and concrete-filled GFRP tube composite cylinders were prepared according to ASTM C 192-90a (Standard Practice for Making and Curing Concrete Test Specimens in the Laboratory) but no rodding or vibration was performed on SCC specimens. All concrete mixtures were prepared using the same mixing sequence in a laboratory rotary mixer. All specimens were moist-cured in a curing room with 100% relative humidity for 27 days, then they were all capped with sulfur caps at both ends and stored at room temperature (about 22 °C) until testing at 91 days from

Table 1
Proportions of concrete mixtures

Mixtures	W/B[a]	Component (kg/m^3)						SP[a] (L/m^3)	VMA[a] (%)	ASHA[a] (L/m^3)
		W[a]	C[a]	FA[a]	GBFS[a]	S[a]	G[a]			
NC[a]	0.45	160	355	–	–	700	1050	–	–	–
SCC[a]	0.45	180	200	80	120	850	850	2	0.04	–
NCE[a]	0.45	155	355	–	–	700	1050	–	–	4
SCCE[a]	0.45	180	200	80	120	850	850	2	0.04	4

[a] See notations.

Table 2
Early-age properties and compressive strength of concrete mixtures

Mixture	Slump (mm)	Slump flow (mm)	Air cont. (%)	Segregation index[a] (%)	L-box flow[a]		f'_c (MPa)	
					h_2/h_1	T_{20} (s)	28-d	90-d
NC	60	–	2.5	–	–	–	34.5	39.5
SCC	–	595	1.3	11.0	0.82	1.6	35.5	43.8
NCE	70	–	1.8	–	–	–	37.0	42.0
SCCE	–	605	1.4	9.0	0.83	1.5	38.5	45.4

[a] Segregation index and L-box flow test methods are explained in Refs. [9,10], respectively.

Table 3
Physical and mechanical properties of GFRP tubes

D^a (mm)	t^a (mm)	α^a	Glass content (%)	Axial direction		Hoop direction		Poison's ratio (v)
				Strength (MPa)	E^a (GPa)	Strength (MPa)	E^a (GPa)	Lateral/ longitudinal
15.0	6.0	±55°	53.5	60.0	8.5	193.0	10.5	0.39

[a] D = inside diameter of the tube, t = thickness of the tube, α = winding angle, E = modulus of elasticity.

Table 4
Properties of short cylindrical specimens prepared for uniaxial compression

Cylinder's type	Concrete mixtures	f'_c (MPa)		No. of confined cylinders	No. of unconfined cylinders	t^a (mm)	D^a (mm)	L^a (mm)
		28-d	90-d					
NC	NC	34.5	39.5	3	3	6	150	300
SCC	SCC	35.5	43.8	3	3	6	150	300
NCE	NCE	37.0	42.0	3	–	6	150	300
SCCE	SCCE	38.5	45.4	3	–	6	150	300
FRP	Hollow	–	–	–	3	6	150	300

[a] f'_c = unconfined concrete compressive strength, t = thickness of FRP tube, D = inside diameter of FRP tube and diameter of unconfined cylinder, L = length of specimen.

casting. Table 4 shows the properties of all cylindrical specimens used for the uniaxial compression test.

The average axial and circumferential strains at mid-height on the exterior surface of each specimen were measured by means of strain gauges. The axial deflection (axial shortening) of each column was measured using an LVDT. Each specimen was instrumented with four 10-mm strain gauges located at its mid-height and attached to its exterior surface. Two gauges were attached in the axial direction at 180° apart to measure the average axial strain and the other two gauges were attached in the circumferential (hoop) direction at 180° apart and 90° from the axial strain gauges to measure the average radial strain as shown in Fig. 1. Plain concrete specimens were coated with epoxy at the location of the strain gauges over an area 10 times larger than the size of the stain gauge. The compression test was performed using a 4600-kN (1035-kips) MTS machine at a loading rate of 4.5 kN/s (1 kip/s) and the axial load was applied to the entire cross-section of the composite cylinder.

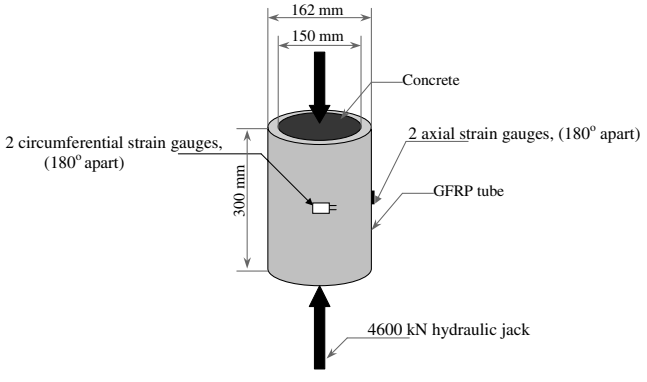

Fig. 1. Illustration of test specimen used in uniaxial compression.

2.2.2. Cylindrical specimens under transverse load

All 150×1100 mm specimens were prepared in a similar manner to the short specimens tested under compression. However, they were moist-cured for 27 days in a curing room at 100% relative humidity and tested at 28-days after casting. Table 5 summarizes the properties of all specimens used for the transverse loading test. All cylinders were instrumented with six 10-mm strain gauges attached to the exterior surface of either the GFRP tube in the confined specimens or the concrete surface in the unconfined ones. The surface of the unconfined concrete specimens at the location of the strain gauges was coated with epoxy over an area 10 times larger than the size of the strain gauge before the gauges were attached. Four strain gauges were installed at the mid-span of each cylinder, two at the top section to measure the average compression strain, and two at the bottom section to measure the average tensile strain. One strain gauge was attached at a distance $d/2$ from each support at the specimen's mid-height and at 45° from the tube's longitudinal axis to measure the average maximum shear strain at that point, (d = the outside diameter of the specimen). The maximum deflection was measured using an LVDT located under the bottom of the central mid-span point (Fig. 2).

All specimens were subjected to transverse load under four-point flexural loading. The distance between the two supports (free span) was 1000 mm (39 in.) and the loading points were 250 mm (9.8 in.) apart in the spec-

Table 5
Properties of cylindrical specimens prepared for flexural test

Cylinder's type	Concrete mixture	f'_c (MPa)		No. of confined cylinders	No. of unconfined cylinders	t^a (mm)	D^a (mm)	L^a (mm)
		28-d	90-d					
BNC	NC	34.5	39.5	3	3	6	150	1100
BSCC	SCC	35.5	43.8	3	3	6	150	1100
BNCE	NCE	37.0	42.0	3	–	6	150	1100
BSCCE	SCCE	38.5	45.4	3	–	6	150	1100
FRP	Hollow	–	–	–	3	6	150	1100

[a] See footnote of Table 3.

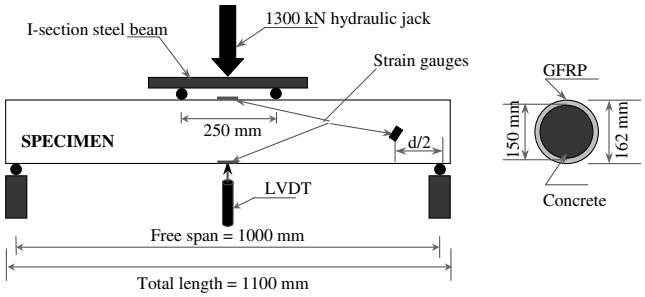

Fig. 2. Illustration of test specimen subjected to transverse load.

imen's mid-section. The applied load was transferred to the specimen through a steel I-section beam resting on two 25-mm (1-in.) diameter steel rollers located at the loading points. Two other 25-mm (1-in.) diameter steel rollers were placed at the supports. Four 10-mm (0.4-in.) thick, 50-mm (2-in.) wide and 162-mm (6.3 in.) inside diameter half-steel rings having an outside rectangular shape were manufactured and rubber-coated to distribute the load to the surface of the cylindrical tube at the loading points and supports. Fig. 2 shows a schematic representation of the transverse load test set-up. The load was applied using a 1300 kN (292 kips) hydraulic jack in a displacement control mode at a rate of 6 mm/min (0.23 in./min) for composite specimens and 0.5 mm/min (0.02 in./min) for the unconfined ones.

3. Results and discussion

The axial load–deformation curves of composite short cylindrical specimens under uniaxial compression can be characterized by three different regions. Two linear stages (first and third regions) connected by a nonlinear transition stage (second region). The first region is dominated by the behavior of the concrete core and the third one is dominated by the behavior of the GFRP tube as shown in Figs. 3 and 4. All confined short specimens behaved similarly during the first and third regions of the loading process. At about 50% of the ultimate load, cracking sounds were heard indicating the progress of failure of the concrete core, followed by a

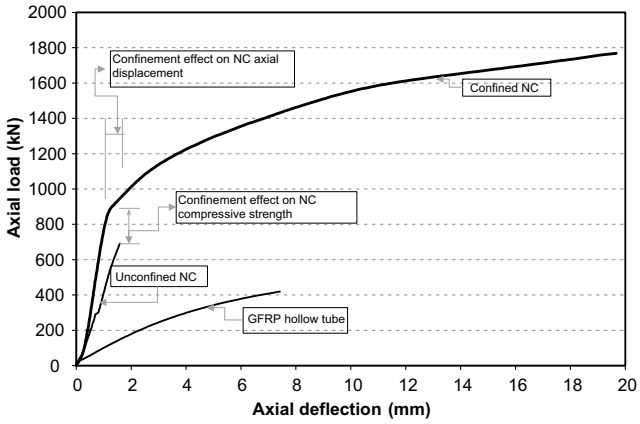

Fig. 3. Axial load–deformation response of NC cylinders and GFRP tube.

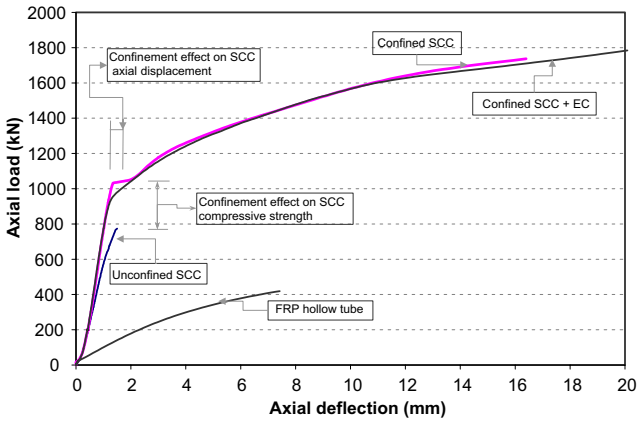

Fig. 4. Axial load–deformation response of SCC cylinders and GFRP tube.

quite steady period during the transition region. White lines started to develop along the fibers at ±55° with respect to the longitudinal axis of the tube at about 60% of the ultimate load, indicating the development of stress in the fibers as shown in Fig. 5. The white colored area along the fibers increased with increasing load to cover most of the middle third of the specimen, leading to fracture of fibers and a sudden failure. For all composite specimens, failure was initiated within the middle third

Fig. 5. Highly stressed area (white lines) along fibers.

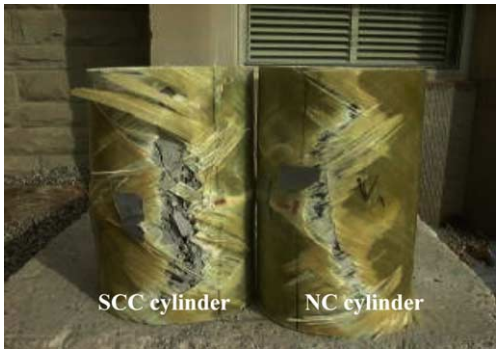

Fig. 6. Typical failure of concrete-filled GFRP tube under uniaxial compression.

of the specimen's height and progressed towards its top and bottom ends. Fig. 6 shows a typical failure mode of a short NC and SCC-filled GFRP tubes under uniaxial compression.

The test results for all short cylindrical specimens subjected to uniaxial compression are summarized in Table 6 (each result is the average value obtained on three identical specimens) and typical axial load–deflection curves for NC and SCC specimens along with that of a hollow GFRP tube are presented in Figs. 3 and 4, respectively. Although the behavior of NC and SCC composite cylinders was comparable, it is clear from both Figs. 3 and 4 that the first region of the composite cylinders' axial load–deformation response coincided with that of unconfined concrete up to 30% and 50% of the unconfined concrete strength for NC and SCC, respectively. However, in both cases (NC and SCC) the confinement effects on concrete strength and axial deformation were similar and equal to 33% (increase) and 13% (decrease), respectively. The confinement effect was calculated as the difference between the concrete strength and axial deformation at failure conditions in confined and unconfined cylinders. The failure of the concrete core in a confined specimen was defined as the point at which the axial load–deformation curve of the composite GFRP-concrete specimen shifted from a linear (stage 1) to a non-linear (stage 2) behavior (Figs. 3 and 4). The ultimate axial-load and axial-deformation of composite cylinders in both cases (NC and SCC) were found to be about 2.5 and 12 times higher than those of unconfined cylinders, respectively. The axial deflection of all column specimens tested under uniaxial compression were measured using an LVDT and the axial deformation values shown were not adjusted for any deformation resulting from the loading platens, ball joint of the testing machine and sulfur caps.

The only significant difference between the behavior of confined NC and SCC cylinders was in the transition region of axial load–deformation curves. Transition between the first and third linear regions in the response of NC was progressive, while for SCC the transition was more sudden as shown in Fig. 7. This indicates that for SCC cylinders there was a short time lag between the

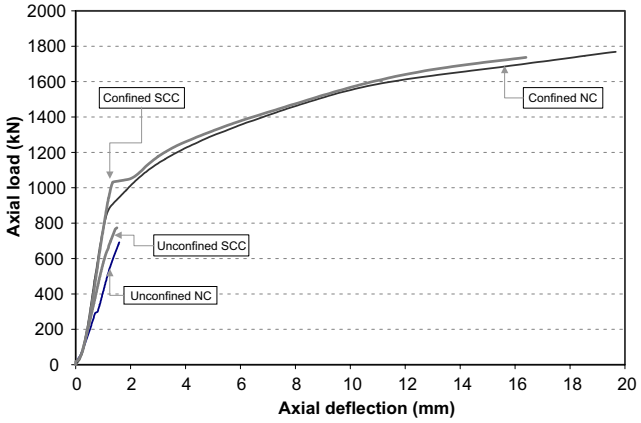

Fig. 7. Axial load–deformation response of NC and SCC cylinders.

Table 6
Test results for short cylindrical specimens subjected to uniaxial compression

Cylinder's type	P_{co}[a] (kN)	P_{cc}[a] (kN)	P_{ult}[a] (kN)	Δ_{co}[a] (mm)	Δ_{cc}[a] (mm)	Δ_{ult}[a] (mm)	$f'cu$[a] (MPa)	ε_{co}[a]	ε_{cu}[a]
NC	690	913	1770	1.59	1.38	19.0	85.8	0.005	0.06
SCC	774	1032	1736	1.50	1.35	16.4	84.2	0.005	0.05
NCE	–	1031	1743	–	1.58	16.7	84.5	–	0.05
SCCE	–	983	1784	–	1.53	20.0	86.5	–	0.06
FRP	–	–	420	–	–	7.4		–	0.02

[a] See notations.

instant when the concrete core failed and when the effect of the GFRP was mobilized. Since the load was applied over the entire cross-section of the composite specimens, the GFRP tube was subjected (after the failure of the concrete core and before concrete was mobilized to restrain the tube from buckling) to a sudden axial load larger than its ultimate strength, which caused a noticeable bulging at the specimen's mid-height.

Typical stress–strain response curves under axial load for plain NC and SCC specimens and concrete-filled GFRP composite specimens are plotted in Fig. 8 in which the first region of the axial stress–strain response of the composite cylinders coincides with the unconfined concrete response in both cases (NC and SCC-filled GFRP tubes). For the same value of axial deformation, the higher axial stress obtained in the case of the SCC-GFRP composite is attributed to the fact that the 91-day compressive strength of plain SCC was slightly higher than that of plain NC. The effect of using expansive cement instead of OPC in NC and SCC is demonstrated in Figs. 9

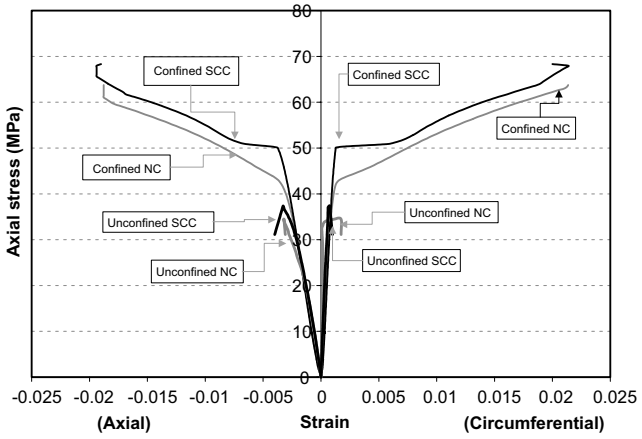

Fig. 8. Stress–strain response of NC and SCC cylinders under uniaxial compression (strain gauges failed at their maximum limit of 0.02).

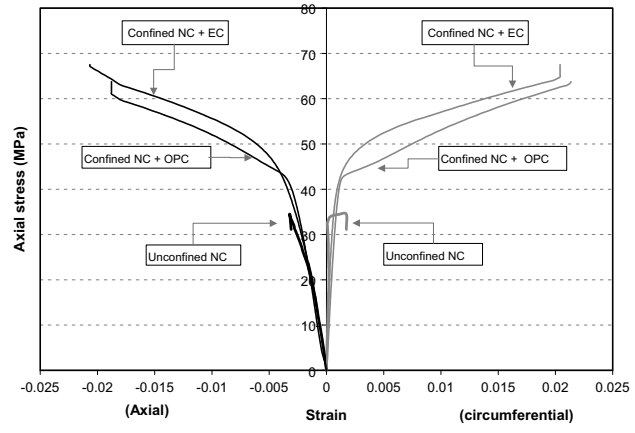

Fig. 9. Stress–strain response of NC and NCE cylinders under uniaxial compression (strain gauges failed at their maximum limit of 0.02).

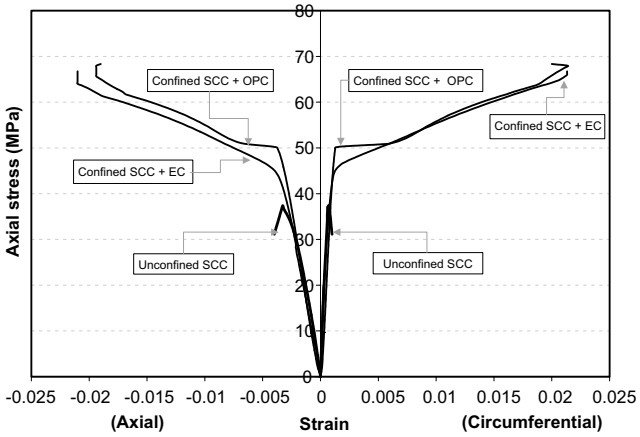

Fig. 10. Stress–strain response of SCC and SCCE cylinders under uniaxial compression (strain gauges failed at their maximum limit of 0.02).

and 10 in which no significant change was observed in the confinement effect on concrete strength and ductility under uniaxial compression. Again the higher stresses in the response curves of NCE (normal concrete with expansive cement) cylindrical specimens are attributed to the fact that the unconfined compressive strength of NCE was slightly larger than that of the unconfined compressive strength of NC.

It is important to investigate the stress–strain relationship of concrete filled GFRP tubes and to examine any differences between the effect of GFRP tube confinement on the behavior of SCC and NC specimens. An analytical model developed by Samaan [4] and Samaan et al. [7] to study the stress–strain relationship of NC columns confined by FRP tubes was applied to results from the present study. The model is presented in the following mathematical form:

$$f_c = \frac{(E_1 - E_2)\varepsilon_c}{\left[1 + \left(\frac{(E_1 - E_2)\varepsilon_c}{f_0}\right)^n\right]^{\frac{1}{n}}} + E_2\varepsilon_c \quad (1)$$

The model expresses the stress (f_c) as a function of the strain (ε_c), the slope of the first and second linear zones of the stress–strain curve (E_1 and E_2, respectively) and a numerical value (n) to control the curvature of the transition zone between zones 1 and 2. Figs. 11 and 12 show the application of the above model to experimental results from the present investigation obtained on NC and SCC short cylindrical specimens, respectively. A good agreement was found in both cases and the model fits the experimental data favorably in the first and third linear zones. However, values of $n = 3.5$ in the case of NC and $n = 5.5$ for SCC were found to be more appropriate than the value of $n = 1.5$ suggested by Samaan [4] and Samaan et al. [7].

The test results for all cylindrical specimens subjected to transverse load are summarized in Table 7 (each

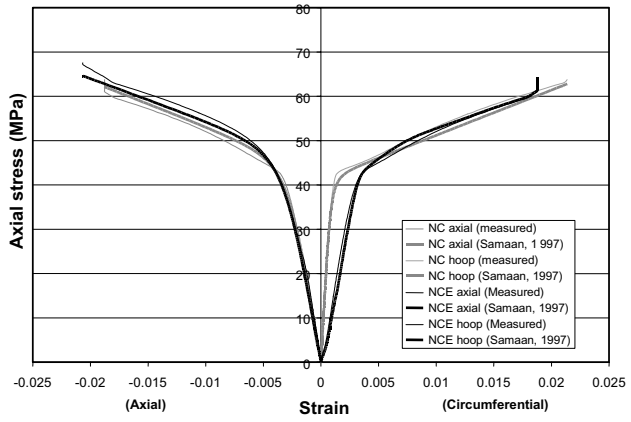

Fig. 11. Stress–strain curve of NC and NCE specimens using the confinement model of Samaan [4].

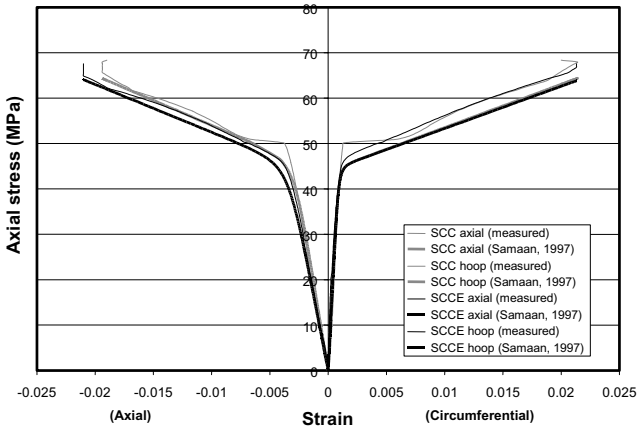

Fig. 12. Stress–strain curve of SCC and SCCE specimens using the confinement model of Samaan [4].

result is the average value obtained on three identical specimens). The load–deflection curves of NC and SCC-filled GFRP composite tubes subjected to transverse load (Fig. 13) can also be characterized by three different regions, as is the case of concrete-filled GFRP tubes under uniaxial compression. However, the strength and stiffness of the GFRP material dominated the behavior of such specimens during the loading process in all three stages. Since no steel was used to reinforce the concrete

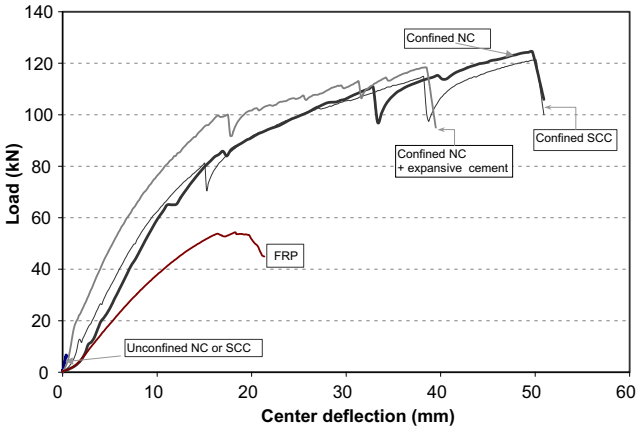

Fig. 13. Load–deflection response of NC and SCC cylinders under transverse load.

core in the unconfined column specimens, their ability to carry transverse load was almost negligible. However, in the case of concrete-filled GFRP composite specimens, the concrete core contributed substantially to the overall strength and ductility. Fig. 13 illustrates typical load–deflection responses of confined and unconfined NC and SCC specimens along with the response of a hollow GFRP tube, all subjected to transverse load. It is shown that the capacity of the GFRP tube in sustaining transverse load increased by 175% from 45 kN (10.2 kips) (ultimate load of hollow tube) to 124 kN (28 kips) (ultimate load of concrete–GFRP composite member) and the maximum deflection of the tube at mid-span was also increased by 133% from 21 mm (0.8 in.) in the case of a hollow tube to 49 mm (2 in.) in the case of an GFRP-concrete composite. Likewise, the ultimate load and maximum deflection at mid-span of the composite specimens subjected to transverse load were found to be 20 and 100 times larger than those of plain concrete specimens, respectively. SCC specimens behaved in a similar manner to that of NC specimens.

Slippage between the concrete core and the GFRP tube may compromise the ultimate load capacity of the composite member, especially under transverse load. Therefore, an attempt was made to strengthen the interfacial contact between the two materials using expansive cement instead of OPC, with the addition of a

Table 7
Test results for cylindrical specimens subjected to transverse load

Cylinder's type	f'_c (28-d) (MPa)	Unconfined specimens		Confined specimens	
		P_{max} (kN)[a]	Δ_{max} (mm)[a]	P_{max} (kN)[a]	Δ_{max} (mm)[a]
NC	34.5	6.5	0.45	124.0	49.7
SCC	35.5	6.1	0.45	121.5	50.0
NCE	37.0	–	–	118.5	39.0
SCCE	38.5	–	–	118.0	53.5
FRP	–	45.0	21.0	–	–

[a] P_{max}, Δ_{max} = maximum transversal load and mid-span deflection of specimen subjected to pure bending, respectively.

shrinkage-reducing admixture. This type of concrete will expand rather than shrink, and therefore can create an active hoop pressure against the internal wall of the GFRP tubes, therefore developing a better contact between the concrete core and the confining tube. The shrinkage-reducing admixture will reduce shrinkage strains, further enhancing this behavior. The performance of specimens prepared with such a concrete is described in Fig. 13. It is shown that in the first and second stages of the response curve and at the same deformation, the load capacity of GFRP tubes filled with concrete using expansive cement is noticeably higher than that of similar tubes filled with concrete made with OPC, indicating that the specimen made with expansive cement was stiffer. However, the ultimate load and deflection of such specimens at failure was slightly lower than those of specimens made using OPC.

An attempt was also made to prevent slippage between the GFRP tube and concrete core by drilling holes through the GFRP tube at 200 mm (7.8 in.) from each of its ends and inserting a 12-mm (0.5 in.) diameter steel bar in each hole before casting the concrete. It was observed during testing that a local failure occurred in the concrete around the steel bars due to stress concentrations, and no major contribution to prevent slippage was noticed (Fig. 14). For all tested specimens, slippage between the concrete and the GFRP at both ends of each specimen varied between 1 mm (0.04 in.) and 3 mm (0.11 in.). During the loading process, it was observed that each time slippage occurred between the concrete and the GFRP, the load dropped, which explains the existence of sudden drops in the load–deflection curves of Figs. 13 and 14. All concrete-filled GFRP tubes shared the same failure mode. White lines along the fibers started to form at mid-span of the bottom section of the GFRP tube and progressed towards the ends. Tensile cracks started to appear on the bottom section of the tube and under both loading points and progressed towards the upper section until a major crack was developed to cause a sudden failure as shown in Fig. 15.

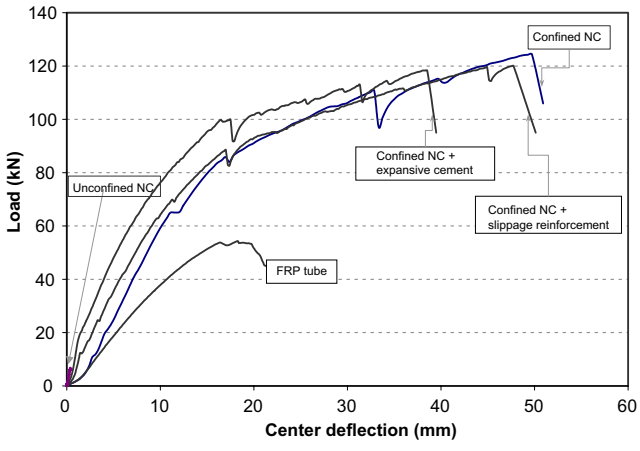

Fig. 14. Effect of expansive cement and slippage reinforcement on load–deflection response of NC cylinders under transverse load.

Fig. 15. Typical failure mode of concrete-filled GFRP tube under transverse load.

While self-consolidating concrete confined in FRP tubes can have several valuable structural applications, there is little data on such applications. Moreover, there is some concern that the often-higher shrinkage associated with SCC and its lower coarse aggregate content compared to that of ordinary concrete could affect its performance under confined conditions. This research shows that confined SCC concrete can achieve similar structural benefits to that of ordinary concrete when confined in GFRP tubes in addition to its ease of construction since no vibration is required for its consolidation.

4. Conclusions

This study investigated the behavior of ordinary and self-consolidating concrete-filled GFRP tubes under both uniaxial compression and transverse loading. Special focus was on: (i) the axial load–deformation and axial stress–strain responses of GFRP tubes filled with either NC or SCC under uniaxial compression; (ii) the load–deformation behavior of such composite tubes under transverse load; and (iii) the effect of using expansive cement and a shrinkage-reducing admixture in concrete on slippage between the GFRP tube and the concrete core. The following conclusions can be drawn from this investigation:

1. SCC-filled GFRP tubes had a comparable behavior to that of NC filled-GFRP tubes under both uniaxial compression and transverse load.
2. The most significant difference between the behavior of NC and SCC-filled GFRP specimens was in the transition region of the response curves, in which the shift from a linear to a non-linear behavior in the load–deformation and stress–strain curves

subsequent to the failure of the concrete core was more sudden for the tested SCC-filled GFRP specimens. However, the use of an expansive cement and a shrinkage-reducing admixture made the behavior of SCC-filled GFRP tubes similar to that of NC-filled GFRP tubes.

3. The use of expansive cement in concrete delayed the occurrence of slippage between the GFRP tube and the concrete core, creating a somewhat better interfacial contact between the two materials, but did not fully prevent slippage. Likewise, the use of localized lateral steel bars placed through the GFRP tube and concrete core did not prevent slippage. Shear connectors or ribs placed inside the GFRP tubes may provide better performance [8].
4. GFRP tube confinement of concrete cylinders increased their ultimate load by 2.5 times and their axial deformation at failure by 12 times under uniaxial compression. It also enhanced their ultimate load by 20 times and their mid-span deflection at failure by 100 times under transverse load.
5. Self-consolidating concrete–GFRP composites offer an easy to construct and corrosion-free alternative to the construction of deep pile foundations, columns, etc. Further research is needed to investigate their large-scale field implementation and performance.

Acknowledgements

The support of the Natural Science and Engineering Research Council of Canada (NSERC) to Professor M. Nehdi was instrumental for the success of this research. M. Nehdi also acknowledges support of the Ontario Innovation Trust and the Canada Foundation for Innovation that allowed creating a state-of-the-art lab in which the research was conducted.

References

[1] Sen R, Shahawy M, Rosas J, Sukumar S. Durability of AFRP and CFRP pretensioned piles in marine environment. In: Non-metallic (FRP) reinforcement for concrete structures, Proceedings of the Third International Symposium, vol. 2, 1997. p. 123–30.
[2] El-Nawawy O, Kandeil A. A new reinforcing material for concrete in the Arabian Gulf. In: Proceedings of the 2nd International Conference on Deterioration and Repair of Reinforced Concrete in the Arabian Gulf, CIRIA, Bahrain, 1987. p. 185.
[3] Mirmiran A, Shahawy M. Behavior of concrete columns confined by fiber composites. J Struct Eng 1997;123(5):583–9.
[4] Samaan MS. An analytical and experimental investigation of concrete-filled fiber reinforced plastics (FRP) tubes. Ph.D. thesis, University of Central Florida, Orlando, FL, 1997. p. 220.
[5] Knowls RB, Park R. Strength of concrete filled steel tubular columns. ASCE, J Struct Div 1969;95(ST12):2565–87.
[6] Mander JB, Park R, Priestly MJN. Theoretical stress–strain model for confined concrete. J Struct Eng, ASCE 1988; 114(8):1804–26.
[7] Samaan M, Mirmiran A, Shahawy M. Model of concrete confined by fiber composites. J Struct Eng 1998;124(9):1025–31.
[8] Mirmiran A, Shahawy M, Samaan M, El Echary H, Mastrapa JC, Pico O. Effect of column parameters on FRP-confined concrete. J Compos Construct 1998;2(4):175–85.
[9] Mitsui K, Yonezawa T, Kinoshita M, Shimono T. Application of new superplasticizer to ultra strength concrete. ACI SP-148, Superplasticizers in concrete, American Concrete Institute, Detroit, Michigan, 1994. p. 27–45.
[10] Fujiwara H. Fundamental study on the self-compacting property of high-fluidity concrete. Proc Japan Concr Inst 1992;14(1):27–32.